DOI: https://doi.org/10.2138/am-2018-6446

REVISION 1

Snapshots of primitive arc magma evolution recorded by clinopyroxene textural and compositional variations: The case of hybrid crystal-rich enclaves from Capo Marargiu Volcanic District (Sardinia, Italy)

Vanni Tecchiato[1,*], Mario Gaeta[1], Silvio Mollo[1,2], Olivier Bachmann[3], Albrecht von Quadt[3], Piergiorgio Scarlato[2]

[1] Dipartimento di Scienze della Terra, Sapienza-Università di Roma, Piazzale Aldo Moro 5, 00185 Roma, Italy

[2] Istituto Nazionale di Geofisica e Vulcanologia, Via di Vigna Murata 605, 00143 Roma, Italy

[3] Institute of Geochemistry and Petrology, ETH Zürich, Clausiusstrasse 25, 8092 Zürich, Switzerland

Corresponding author:
Dr. Vanni Tecchiato
Department of Earth Sciences
Sapienza - University of Rome
P.le Aldo Moro 5
00185 Roma -Italy
Tel. 0039 – 0649914916
Email: vanni.tecchiato@uniroma1.it

ABSTRACT

Capo Marargiu Volcanic District (CMVD) is an Oligo-Miocene calc-alkaline complex located in north-western Sardinia (Italy) and characterized by the widespread occurrence of basaltic to andesitic domes. One of these domes hosts abundant crystal-rich enclaves with millimeter-to-centimeter-sized clinopyroxenes showing intriguing textural features as a result of complex magma dynamics. To better understand the mechanisms governing the early evolution of the CMVD magmatic system, such clinopyroxene phenocrysts have been investigated in terms of their major, trace element and isotopic compositions. Three distinct clinopyroxene populations have been identified, i.e., Type 1, Type 2, and Type 3. Type 1 appears as the sub-rounded cores of diopsidic clinopyroxenes with overgrowth textures corresponding to Type 2 and Type 3. These latter populations may also occur as single isolated crystals. Type 2 diopsidic pyroxene exhibits oscillatory zoning and spongy cellular textures with Type 3 overgrowths, whereas Type 3 are polycrystalline augitic glomerocrysts with occasional Type 2 overgrowths. The crystal overgrowths are striking evidence of magma recharge dynamics. Type 1 ($^{cpx}Mg\#_{83\text{-}92}$), Type 2 ($^{cpx}Mg\#_{75\text{-}82}$) and Type 3 ($^{cpx}Mg\#_{72\text{-}79}$) are, respectively, in equilibrium with Sardinian mantle-derived high-Mg basalts (HMB with $^{melt}Mg\#_{56\text{-}73}$), least differentiated basaltic andesites (BA with $^{melt}Mg\#_{45\text{-}56}$) and evolved basaltic andesites (EBA with $^{melt}Mg\#_{41\text{-}50}$). Type 1 and Type 2 are diopsidic phenocrysts which have evolved along a similar geochemical path (i.e., linear increase of Al, Ti, La, and Hf contents, as well as negligible Eu-anomaly) controlled by olivine + clinopyroxene + amphibole fractionation. This differentiation path is related to phenocryst crystallization from hydrous HMB and BA magmas stalling at moderate crustal pressures. The occurrence of globular sulfides within Type 1 suggests saturation of the HMB magma with a sulfide liquid under relatively low redox conditions. Moreover, Type 1 clinopyroxenes show variable $^{87}Sr/^{86}Sr$ ratios ascribable either to assimilation of crustal material by HMB magma or a mantle source variably contaminated by crustal components. In contrast, Type 3 augitic phenocrysts recorded the effect of

plagioclase and titanomagnetite fractionation (i.e., low Al and Ti contents associated with high La and Hf concentrations, as well as important Eu-anomaly) from more degassed EBA magmas ponding at shallow depths. Rare titanite associated to Type 3 and titanomagnetite crystals point to high oxidizing conditions for EBA magmas. The $^{87}Sr/^{86}Sr$ ratios of both Type 2 and Type 3 are almost constant, suggesting a limited interaction of BA and EBA magmas with the country rock. The overall textural and compositional features of Type 1, Type 2 and Type 3 clinopyroxene phenocrysts lead to the conclusion that CMVD was characterized by a polybaric plumbing system where geochemically distinct magmas crystallized and mixed under variable environmental conditions.

Keywords: clinopyroxene phenocrysts, overgrowth textures, Sr-isotopes, trace elements, high-Mg basalts, Sardinian magmatism.

INTRODUCTION

Igneous rocks crystallized from arc magmas may show complex textural and compositional features that potentially reflect the intricate processes controlling the solidification path of the system. For example, during ascent of magma from the deep source region to a shallow storage reservoir, puzzling phenocryst textures and zoning patterns may result from resorption and remobilization phenomena (Pyle et al. 1988; Turner et al. 2003; Dungan and Davidson 2004), as well as from convection in a thermally and chemically zoned magma chamber (Singer et al. 1995). In arc environments, the labyrinthine architecture of the volcanic plumbing system can exert a primary control on magma evolution, implying that different magma bodies evolve separately and then eventually interact via mingling and mixing processes (e.g., Anderson 1976; Eichelberger 1980; Clynne 1999). The mineral texture of hybrid products will ultimately depend on the degree of interaction between the two end-member magmas, responding to the effect of melt viscosity (e.g., Sparks and Marshall 1986; Jellinek et al. 1999), bulk composition (Sparks and Marshall 1986), and involved melt volume (Nakagawa et al. 2002; Streck et al. 2002; Humphreys et al. 2013). However, recharge events in shallow magma reservoirs may be cryptic and difficult to detect if only the bulk rock analyses are taken into account (e.g., Streck et al. 2002; Humphreys et al. 2006). In contrast, mineral textural and compositional variations can faithfully document the magmatic history of the system (e.g., D'Lemos 1996; Humphreys et al. 2006; Frey and Lange 2011). Among the most common mineral phases, clinopyroxene nucleates and grows under a wide spectrum of crystallization conditions, recording the pressure (Putirka 2008; Neave and Putirka 2017), temperature (Putirka et al. 2003; Putirka 2008), melt-water content (Armienti et al. 2013; Perinelli et al. 2016), and oxygen fugacity (France et al. 2010) of the system. This is especially true for the case of mafic to intermediate arc magmas, where the clinopyroxene-in temperature varies from the liquidus of high-pressure basaltic/picritic melts (e.g., Melekhova et al. 2015) to the sub-aerial solidus of the eruptive magmas (e.g., Baker and Eggler 1987; Grove and Juster 1989). In this framework, major and trace element zoning patterns, as well as stable and radiogenic isotope concentration in clinopyroxene are used to retrieve important information on: (i) the mantle source of primitive arc products (e.g., Sas et al. 2017), (ii) mixing processes between compositionally distinct magmas (e.g., Nakagawa et al. 2002; Streck et al. 2002), (iii) crystal mush remobilization phenomena (e.g., Forni et al. 2016), and (iv) extensive assimilation of the country rock by magma (e.g., Gaeta et al. 2009; Di Rocco et al. 2012).

The Capo Marargiu Volcanic District (CMVD) is a calc-alkaline complex located in north-western Sardinia (Italy) and is characterized by the occurrence of basaltic to andesitic domes and dikes. Magma dynamics at CMVD were controlled by fractional crystallization, country rock assimilation, and crystal recycling in polybaric environments (Tecchiato et al. 2018). In this study, we present major, trace element and isotopic compositions of millimeter-to-centimeter-sized clinopyroxene phenocrysts from crystal-rich enclaves found in the lava domes at CMVD. The intriguing zoning patterns and complex geochemical variations of clinopyroxenes provide new insights into the mechanisms governing the early evolution of the magmatic system and give evidence of a complex interplay between Sardinian magmas and the continental crust stretched by back-arc tectonics.

GEOLOGICAL SETTING

The late Mesozoic-Cenozoic eastward to southward migration of the Apennine-Maghrebide fold-and-thrust belt (Carminati et al. 2012; Lustrino et al. 2004, 2009), at the subduction-collisional boundary between the upper European and the lower Ionian and Adria plates, caused (i) the back-arc stretching and boudinage of the European margin, (ii) the formation of a series of V-shaped basins and (iii) the ultimate isolation of lithospheric ribbons in the middle of Central-Western Mediterranean area (Carminati et al. 2012, and references therein). The islands of Sardinia and Corsica represent a thin slice of the European continental block between the Ligurian-Provençal and Tyrrhenian oceanic basins, left behind after a ~55-60° counter-clockwise rotation lasting from Late Oligocene to Early Miocene (Cherchi et al. 2008; Dieni et al. 2008, and references therein). Therefore, during the time span between Late Eocene - Early Miocene (Lustrino et al. 2009), the geodynamic evolution was accompanied by the widespread production of subduction-related magmas with both tholeiitic and calc-alkaline affinities. The earliest manifestation of this magmatic phase (~38 Ma) was the microdioritic body of Calabona (north-western Sardinia), interpreted as the result of anatexis phenomena within the Hercynian lower crust (Lustrino et al. 2009). This event was chronologically isolated from the peak of productivity (22-18 Ma) recorded by the thick volcanic sequences erupted throughout the north-south Fossa Sarda graben (Lecca et al. 1997; Lustrino et al. 2004, 2009). This intense magmatism was triggered and fed by processes of mantle hydration via slab-derived fluids (Franciosi et al. 2003; Lustrino et al. 2013) coupled with adiabatic upwelling of asthenosphere (Mattioli et al. 2000; Franciosi et al. 2003; Carminati et al. 2012). Indeed, incompatible trace element variations in tholeiitic and calc-alkaline basalts to rhyolites show the typical subduction-related geochemical signature of arc magmas (e.g., Duggen et al. 2005; Avanzinelli et al. 2009; Lustrino et al. 2011), with chondrite-normalized patterns showing LREE-enrichments and HREE-flattening, due to a metasomatised spinel-bearing mantle source (Brotzu et al. 1997b; Morra et al. 1997; Downes et al. 2001; Franciosi et al. 2003; Lustrino et al. 2009). The variation of Nd-Sr isotopes relative to SiO_2 has been interpreted to reflect three main processes: (1) interaction between mantle magmas and crustal material (Morra et al. 1997; Franciosi et al. 2003; Lustrino et al. 2013), (2) re-melting of early underplated and solidified mafic rocks (Lustrino et al. 2013), and (3) mixing between crustal-contaminated and anatectic magmas (Lustrino et al. 2013).

At the scale of a single volcanic district, such as Sarroch (Conte et al. 1997), Sant'Antioco (Conte et al. 2010), Narcao (Brotzu et al. 1997a), Arcuentu (Brotzu et al. 1997b), Sindia (Lonis et al. 1997), and Montresta (Morra et al. 1997), mafic to intermediate products generally delineate multiple differentiation trends. These geochemical variations have been mostly ascribed to the segregation of either "dry" or "wet" solid assemblages from compositionally heterogeneous progenitors crystallizing in polybaric environments (e.g., Brotzu et al. 1997a, 1997b; Conte et al. 1997; Lonis et al. 1997). A similar scenario is in agreement with the syntectonic character of the magmatic system interacting with a crustal environment affected by extensive structural deformation (Lecca et al. 1997; Mattioli et al. 2000). Additionally, the presence of xenocrystic materials, plutonic textured enclaves, and cognate polycrystalline aggregates in the eruptive products confirms that fractional crystallization was the principal mechanism driving Sardinian magmatism.

In north-western Sardinia (i.e., Logudoro-Bosano domain; Fig. 1a) four eruptive sequences have been identified: lower andesitic, lower ignimbritic, upper andesitic, and upper ignimbritic series (Coulon and Baque 1973; Coulon et al. 1978; Deriu 1964). The volcanic succession is therefore structured as alternating units of bimodal compositions, corresponding to either basalt/andesite (andesitic series) or dacite/rhyolite (ignimbritic series). In addition, rare high-Mg basaltic rocks, representing the most primitive products of the island (Morra et al. 1997), are also found at Montresta (Fig. 1a), ~10 km northeast of CMVD. Geochronological studies conducted with the K-Ar method constrained the four eruptive sequences between 24 ± 1.2 Ma (Montigny et al. 1981) and 16.3 ± 1.0 Ma (Coulon et al. 1974). The CMVD stratigraphy is dominated by the lower andesitic series (Fig. 1b), as large volumes of basaltic andesitic domes and andesitic autoclastic lava flows (cf. Deriu 1964; Lecca et al. 1997). Late stage andesitic dikes and sills pervasively intrude these formations. Importantly, on the coast of Cala Bernardu (Fig. 1b), a cliff exposes the inner part of a basaltic andesitic dome hosting abundant crystal-rich enclaves (Fig. 1c). The dome appears as a yellowish, porphyritic rock with ~15% of phenocrysts, whereas the dark-grey enclaves are centimeter-to-meter-sized rounded blocks with ~50% of coarse-grained crystals (Fig. 1d). From a mineralogical, petrological, and geochemical point of view, the crystal-rich enclaves, basaltic andesitic domes, and andesitic dikes have been described in detail by Tecchiato et al. (2018) and, therefore, they are only briefly summarized in this study.

SUMMARY OF ENCLAVE PETROLOGY

Enclaves are crystal-rich, porphyritic rocks containing ~40-50% of coarse grained diopsidic to augitic clinopyroxene + Mg-hastingsitic amphibole + anorthitic to bytownitic plagioclase + Fo_{66-87} olivine + titanomagnetite ± Cr-spinel (in order of abundance). The millimeter-to-centimeter-sized minerals are dispersed in a microcrystalline groundmass of bytownitic to andesinic plagioclase + augitic clinopyroxene + titanomagnetite ± low-Ca pyroxene ± titanite. Coarse-grained diopside and Mg-hastingsite show complex textures (i.e., dissolution features and reaction rims) that reflect sharp disequilibrium effects resulting from open-system magma dynamics ascribable to entrainment of early-formed crystals in a compositionally distinct melt (Tecchiato et al. 2018). While olivine (Fo_{84-87}) and clinopyroxene ($Mg\#_{83-92}$) phenocryst cores equilibrated with a high-Mg basaltic magma ($Mg\#_{64-65}$) progenitor of the CMVD stratigraphic succession, the groundmass crystallization was controlled by the input of basaltic andesitic to andesitic magmas compositionally similar to lava domes and dikes (Tecchiato et al. 2018).

The hybrid nature of crystal-rich enclaves is also confirmed by bulk rock chemical data. Enclaves are high-Mg basalts (9.3–10.7 wt% MgO and 46.0–48.6 wt% SiO_2) with low Cr (186-338 ppm) and Ni (26-133 ppm) contents and high Sc (74-81 ppm) and V (457-470 ppm) concentrations in contrast to the typical mantle derived products erupted in Sardinia (i.e., Cr = 186-739 ppm, Ni = 47-226 ppm, Sc = 42-51 ppm, V = 261-318 ppm; cf. Morra et al. 1997). Moreover, primordial mantle-normalized incompatible trace element patterns of enclaves (e.g., La_N = 11.7-13.5, Ba_N = 27.3-55.5, Nb_N = 3.5-5.8) closely match with those (i.e., La_N = 10.0-27.7, Ba_N = 17.2-36.1, Nb_N = 4.5-14.0; cf. Morra et al. 1997) of more evolved basaltic to basaltic andesitic rocks erupted at Montresta (Fig. 1a).

Major and trace element modeling reveals that the coarse-grained assemblage of enclaves corresponds to the cumulitic horizon segregated during magma differentiation of the high-Mg basaltic progenitor to produce basaltic andesitic compositions (Tecchiato et al. 2018). During the emplacement of the basaltic andesitic dome, further melt infiltrated, disaggregated and reacted within the cumulate horizon, carrying ~50% of the early-formed material (Tecchiato et al. 2018).

METHODS

Enclave specimens were crushed to centimeter-sized fragments using a mechanic mill and then further disaggregated through a high voltage pulse power system. The resulting natural shaped clinopyroxenes and clinopyroxene fragments were hand-picked and set in 1-inch epoxy mounts for polishing.

Major element analyses of clinopyroxene (Tabs. S1-S3) were carried out with a Jeol-JXA8200 electron probe micro analyzer (EPMA) installed at the HPHT Laboratory of Experimental Volcanology and Geophysics of the Istituto Nazionale di Geofisica e Vulcanologia (INGV) in Rome, Italy. The accelerating voltage and beam current were 15 kV and 10 nA, respectively. The beam size was 5 μm with a counting time of 20 and 10 s on peaks and background, respectively. The following standards have been adopted for the various chemical elements: wollastonite (Si and Ca), jadeite (Na), corundum (Al), forsterite (Mg), andradite (Fe), rutile (Ti), orthoclase (K), spessartine (Mn) and chromite (Cr). The precision of the microprobe was measured through the analysis of well-characterized synthetic oxides and minerals. Data quality was ensured by analyzing these test materials as unknowns following Iezzi et al. (2014).

Images were collected at the INGV using the backscattered electron (BSE) mode of a field emission gun-scanning electron microscopy (FE-SEM) Jeol 6500F equipped with an energy-dispersive spectrometer (EDS) detector.

Trace element concentrations in clinopyroxene were determined by laser ablation inductively coupled plasma mass spectrometry (LA-ICPMS) using a 193 nm Resonetics ArF excimer laser coupled with a Thermo Element XR ICP mass spectrometer at the Institute of Geochemistry and Petrology, ETH Zürich. The following geochemical groups were analyzed: (i) rare earth elements (REE), including light rare earth elements (LREE; i.e., La, Ce, Pr, Nd), middle rare earth elements (MREE; i.e., Sm, Eu, Gd, Tb, Dy), and heavy rare earth elements (HREE; i.e., Ho, Er, Tm, Yb, Lu, Y), (ii) large ion lithophile elements (LILE; i.e., K, Rb, Sr, Cs, Ba), and (iii) high field strength elements (HFSE; i.e., Zr, Nb, Hf, Ta). The spot size was 29 μm and the output energy of the laser beam was typically ~3.5 J/cm^2. The MATLAB-based program SILLS (Guillong et al. 2008) was employed to calculate element concentration ratios using signal intensities obtained from NIST612/NIST610 silicate glasses as external standards measured twice every 25-30 spots to correct for drift. For each data point, the resulting ratios were converted to absolute concentrations using the internal standard of CaO content previously acquired from EPMA analyses. USGS reference glass GSD-1G was used as secondary standard to monitor the accuracy of the instrument. The precision of a single spot analysis is difficult to quantify, but replicate analyses of a homogeneous mineral or glass give precisions for element concentrations ≫LOD (limit of detection) better than 5% of the value.

Selected crystals were cut along the boundary between adjacent chemical zones using the 193 nm Resonetics ArF excimer laser. The spot size and the output energy of the laser beam adopted were 73 μm and ~4.5 J/cm^2, respectively. Prior to cutting, thick (~300-400 μm) sections of the epoxy mounts were prepared with the aim of regularizing crystal geometry and exerting an accurate control on zoning pattern propagation in the inner part of crystal. This improved the precision of our technique by lowering the probability that unwanted remnants of a chemical zone remained embedded in the adjacent portion after cutting. Clinopyroxene portions were sufficiently large (>$6\cdot10^{-2}$ mm^3) and rich in Sr (~20-25 ppm) to ensure a minimum quantity of ~3 ng of Sr (cf. Ramos and Tepley 2008) necessary for $^{87}Sr/^{86}Sr$ measurements by thermal ionization mass spectrometry (TIMS). Crystals were digested with a concentrated HF/HNO_3 mixture for 3 days. After evaporation, the material was re-dissolved in 2.5 N HNO_3, followed by Sr separation in PP ion exchange columns with Sr-spec resin, according to the chromatography technique of Pin et al. (1994). Strontium isotope ratios were measured on a Thermo TRITON Plus multicollector TIMS at ETH Zürich in static mode. The Sr isotope ratios are mass fractionation corrected to $^{88}Sr/^{86}Sr$ = 8.375209. The NBS 987 standard measurements returned $^{87}Sr/^{86}Sr$ = 0.7103050 ± 0.0000079 (2 se; n = 14) during the period of analysis.

CLINOPYROXENE ZONING PATTERNS

Mineral textural (Figs. 2, 3, and 4) and compositional (Tabs. S1-S3) features discriminate three distinct clinopyroxene populations, i.e., Type 1, Type 2, and Type 3. Type 1 appears as the core of large (> 1 mm in size) clinopyroxenes with overgrowth textures corresponding to Type 2 and Type 3 populations (Fig. 2) that, however, may also occur as single isolated crystals. Type 1 shows disequilibrium dissolution features (Fig. 2a and b), predominantly sub-rounded edges (Fig. 2a), and rare spongy cellular textures associated with patchy zoning (cf. Tecchiato et al. 2018). These crystals usually contain globular inclusions of Fe + Ni + Co sulfides, that likely represent drops of an immiscible liquid (Fig. 2c). Type 2 occurs as millimeter-sized crystals with a weak reverse oscillatory zoning (Fig. 3a and c) or, alternatively, a spongy cellular texture associated with thick (0.1 - 0.5 mm) Type 3 overgrowths (Fig. 3b). In some cases, Fo_{75-79} olivine is included in Type 2 that, in turn, may be entrapped by large amphibole crystals with $Mg\#_{73-76}$ (Fig. 3c). Type 3 is typically found as millimeter-sized glomerocrysts together with plagioclase (An_{88-93}), titanomagnetite (Usp_{20-40}) and rare Fo_{66-67} olivine (Fig. 4a and b). These clinopyroxenes occasionally show Type 2 overgrowths (Fig. 4c).

According to Morimoto (1988), Type 1 and Type 2 are diopside (Wo_{44-47}-En_{44-50}-Fs_{5-9} and Wo_{45-48}-En_{40-44}-Fs_{9-14}, respectively), whereas Type 3 is augite (Wo_{41-45}-En_{41-45}-Fs_{12-16}). The Al_{tot} vs. Mg-number [Mg# = 100 · Mg/(Mg + Fe_{tot})] and Ti diagrams (Fig. 5) show that Type 1 and Type 2 evolve along a similar path controlled by olivine + clinopyroxene + amphibole fractionation (Fig. 3c and d). As a consequence, Al_{tot} and Ti increase, respectively, from 0.081 to 0.383 apfu and from 0.006 to 0.037 apfu, whereas Mg# decreases from 93 to 75. In contrast, Type 3 appears as an isolated group recording the effect of plagioclase fractionation (Fig. 4a and b). The more evolved character of the magma causes Al_{tot} and Mg# in Type 3 to reach minimum values of 0.111 apfu and 72, respectively. This observation is also confirmed by the Zn vs Eu/Eu* (Eu_N/ [$\sqrt{(Sm_N)} \times \sqrt{(Gd_N)}$]) diagram (Fig. 6a), showing strong (0.71–0.82) and weak (0.80–1.01) Eu anomalies for Type 3 and for Type 1 + Type 2, respectively. Similarly, the Y vs. Zr diagram (Fig. 6b) shows that Type 3 (plagioclase-dominated environment) is characterized by much higher concentrations of incompatible trace elements relative to Type 1 + Type 2 (olivine + clinopyroxene + amphibole -dominated environment). The REE chondrite-normalized patterns (Fig. 7) for Type 1, Type 2 and Type 3 are bell-shaped, showing relative depletions in both LREE and HREE with respect to MREE. The REE concentrations increase from Type 1 + Type 2 to Type 3, according to the more differentiated character of the magma. The Sr isotopic composition of

Type 1 shows highly variable $^{87}Sr/^{86}Sr$ ratios (0.705815-0.707344) at the early stage of magma differentiation controlled by olivine + clinopyroxene fractionation (Fig. 8). In contrast, the $^{87}Sr/^{86}Sr$ ratios remain almost constant for Type 2 and Type 3 (0.706825-0.707286), at the late stage of magmatic evolution.

DISCUSSION

Magma differentiation processes

According to a number of studies (Dobosi 1989; Simonetti et al. 1996; Cioni et al. 1998; Morgan et al. 2004; Mollo et al. 2010; Forni et al. 2016), the compositional variation of clinopyroxene closely reflects the physicochemical changes of the magmatic reservoir under the effects of both closed- and open-system processes (i.e., magma mixing/mingling, mush rejuvenation, and crust assimilation). Thus, major and trace element analyses of Type 1, Type 2, and Type 3 are potential sources of information on the mechanisms driving the differentiation of CMVD magmas in different P-T-X-H_2O environments.

As a first approach, the compositions of the melts hypothetically in equilibrium with the distinct clinopyroxene populations have been derived by applying the clinopyroxene-melt Fe-Mg exchange reaction [$^{cpx\text{-}melt}Kd_{Fe–Mg} = (Fe^{cpx} / Fe^{melt}) \times (Mg^{melt} / Mg^{cpx})$] proposed by Putirka (2008). Using a value of 0.27 ± 0.03, results from calculations suggest the attainment of equilibrium crystallization between Type 1 ($^{cpx}Mg\#_{83\text{-}92}$) and mantle-derived high-Mg basalts (HMB with $^{melt}Mg\#_{56\text{-}73}$; e.g., Montresta, Arcuentu, and Marmilla products), Type 2 ($^{cpx}Mg\#_{75\text{-}82}$) and least differentiated basaltic andesites (BA with $^{melt}Mg\#_{45\text{-}56}$; e.g., Arcuentu and Sarroch products), and Type 3 ($^{cpx}Mg\#_{72\text{-}79}$) and more evolved basaltic andesites (EBA with $^{melt}Mg\#_{41\text{-}50}$; e.g., Montresta, Sindia, and Sant'Antioco products). These mineral-melt equilibria indicate that the coexistence of Type 1, Type 2, and Type 3 from crystal-rich enclaves reflects open-system pre-eruptive crystallization conditions, as well as indicating that magma differentiation and magma mixing were the most important mechanisms contributing to the geochemical evolution of the plumbing system, as typically observed for a variety of subduction-related arc settings with calc-alkaline affinity (cf. Scarlato et al. 2017, and references therein).

The linear increase of Al_{tot} from Type 1 to Type 2 (Fig. 5) is related to the differentiation of HMB towards BA, responding to the fractionation of mafic mineral phases. This is consistent with the small Eu-anomaly of Type 1 + Type 2 (0.80–1.01) coupled with the low concentrations of Zn (14-41 ppm; Fig. 6). Previous experimental studies (Pichavant and Macdonald 2007; Melekhova et al. 2015) have recognized that, under high pressure and hydrous conditions, the differentiation of primitive arc magmas (i.e., HMB) located at the base of the crust is mostly driven by olivine + clinopyroxene + amphibole segregation, whereas plagioclase crystallization is suppressed. Importantly, Type 2 compositions (6.2-8.6 wt% Al_2O_3) have been experimentally derived by Melekhova et al. (2015) for clinopyroxenes (4.2-8.1 wt% Al_2O_3) formed from high-Al basaltic melts (14.6-17.9 wt% Al_2O_3) equilibrated at P = 0.7-1.0 GPa, T = 1030-1150 °C, H_2O = 5.3-9.7 wt%, and fO_2 = NNO – NNO+4. Additionally, barometric, thermometric, hygrometric, and oxygen barometric estimates conducted on the CMVD products by Tecchiato et al. (2018) provide constraints on the crystallization of high-Mg basaltic to basaltic andesitic magmas at 0.5-0.7 GPa, 1030-1180 °C, 5-6 wt% H_2O, and NNO – NNO+2. Large amphibole crystals associated with Type 2 clinopyroxenes (Fig. 3d) and olivines (Fig. 3c) testify to H_2O-rich environments where plagioclase crystallization is delayed and possibly suppressed. From Type 1 to Type 2, the significant decrease of transition elements (i.e., Cr = 11-4628 ppm) with increasing concentrations of incompatible elements (i.e., Zr = 0.4-27.7 ppm) suggests early and extensive crystallization of mafic minerals (e.g., Cr-spinel + clinopyroxene + amphibole) in which Cr is prevalently incorporated (Tabs. S1-S3). In contrast, the low Al_{tot} content (Fig. 5), the evident Eu-anomaly and the high Zn concentration (Fig. 6) of Type 3 reflect clinopyroxene and plagioclase cosaturation from EBA magmas (Figs. 4a and b). Specifically, the incorporation of Zn into clinopyroxene structure is highly influenced by the activity of Ca in the melt (Gori et al. 2015). This implies that Ca fully occupies the clinopyroxene M2 site, forcing Zn to enter the M1 site in six-fold coordination. Since Zn preferentially assumes a four-fold coordination (Neumann 1949), it readily enters the M2 site becoming strongly compatible into clinopyroxene as soon as Ca-activity in the melt decreases and calcium is unable to buffer this site. In this situation, Zn is accepted in the more appropriate four-fold coordination when the structural deformation is easily accommodated by the highly flexible M2 site (Gori et al. 2015). The onset of plagioclase crystallization indirectly lowers the activity of Ca in the melt, favoring Zn incorporation into the Type 3 crystal lattice.

The Fe_{tot}^{+2} vs. ΣTs (Ca-Tschermak + CaFe-Tschermack + CaTi-Tschermak) diagram (Fig. 9) shows that Type 1 + Type 2 describe a positive trend, as the result of HMB differentiation towards BA magmas along a path of increasing H_2O. Indeed, Dolfi and Trigila (1978) have experimentally investigated the compositional effect produced by water dissolved in the melt on clinopyroxene, demonstrating that ΣTs and Fe linearly increase (from 0.22 to 0.27 and from 0.29 to 0.41, respectively) when the melt Si-activity and Fe^{+2}/Fe^{+3} ratio become lowered under increasingly hydrous conditions (from 2.2 to 3.5 wt% H_2O). High water contents are known to (1) depress the saturation surface of plagioclase, expanding the stability field of olivine, clinopyroxene, and amphibole (Sisson and Grove 1993; Melekhova et al. 2015), and (2) shift the crystallization temperature of spinel close to the liquidus of basaltic magmas (Berndt et al. 2005). Thus, Type 1 + Type 2 clinopyroxenes with Ca-Al-rich, Fe-poor compositions preferentially crystallize from HMB + BA magmas, accounting for the lack of plagioclase and the early fractionation of spinel. Conversely, Type 3 and plagioclase cosaturation characterizes the more degassed EBA magmas, likely ponding in upper crustal reservoirs. Tecchiato et al. (2018) have estimated that Type 3 clinopyroxenes equilibrate at *P* and H_2O conditions (i.e., 0.1-0.4 GPa and 1-3 wt%, respectively) distinctly lower than those of Type 1 + Type 2 (i.e., 0.7-1.0 GPa and 5.3-9.7 wt%, respectively). The same finding can be extended to other volcanic districts in Sardinia

(Fig. 9), according to the similar compositional features shared by Type 3 clinopyroxenes and the natural phenocrysts found in basaltic to andesitic products from Sarroch (Conte et al. 1997), Narcao (Brotzu et al. 1997a), Arcuentu (Brotzu et al. 1997b) and Sindia (Lonis et al. 1997).

The Al^{IV} vs. La and Hf diagrams (Fig. 10) confirm that Type 1 + Type 2 evolve along an almost linear path, depicting the progressive differentiation of HMB to BA magmas. It has been commonly documented in literature that the incorporation of REE (+3 cations) into the clinopyroxene structure is positively correlated with Al^{IV}, responding to the increased ease of locally balancing the excess charge at M2 site as the number of surrounding tetrahedral Al atoms increases (Hill et al. 2000; Wood and Blundy 2001; Wood and Trigila 2001; Tuff and Gibson 2007; Sun and Liang 2012; Mollo et al. 2013a, 2016, 2017; Bedard 2014; Scarlato et al. 2014). This conforms to the differentiation of Type 1 + Type 2 that is mostly controlled by the exchange equilibria between Ca-Tschermak (CaTs) and Diopside + Hedenbergite (DiHd), where the volume changes for the solution of CaTs into DiHd are significantly low, leading to a temperature-dependent reaction (Putirka et al. 1996; Putirka 2008; Mollo et al. 2013b). Consequently, as the temperature of the system decreases driving melt differentiation, REE contents in clinopyroxene increase through the exchange of ^{M2}Mg with ^{M1}Al coupled with the substitution of Si with Al in the tetrahedral site to form CaTs (Fig. 10). Similarly, HFSE (+4 and +5 cations) are more easily accepted into the clinopyroxene crystal lattice when this coupled substitution causes a charge deficiency in the tetrahedral site and the increase of M1 site average charge (Hill et al. 2000; Wood and Trigila 2001; Marks et al. 2004; Mollo et al. 2013a, 2016, 2017). Thus, Type 3 forms an isolated group of data characterized by low Al^{IV} and high Hf and La concentrations (Fig. 10) due to clinopyroxene crystallization from a geochemically distinct magma (i.e., EBA) that equilibrated at shallower and more degassed conditions in a plagioclase-dominated environment (Fig. 6).

Magma redox state

Textural evidence directly ascribable to magma redox conditions can be accounted for by fO_2 variations from HMB + BA to EBA magmas. The occurrence of globular sulfides within Type 1 (Fig. 2c) suggests saturation of HMB melt with a sulfide liquid (cf. Hattori 1996). Depending on magma fO_2 conditions, sulfur is found either as S^{2-} (with minor HS^-) or as $(SO_4)^{2-}$ (Katsura and Nagashima 1974; Carroll and Rutherford 1988). According to Carroll and Rutherford (1988), the redox boundary of dissolved sulfur species is one log fO_2 unit above the NNO buffer. Therefore, globular sulfides within Type 1 indicate that S^{2-} is the predominant sulfur species dissolved in the HMB, testifying to oxygen fugacity below NNO+1 (e.g., Parat et al. 2011). These estimates match with those provided by Morra et al. (1997) for Montresta HMB (NNO – NNO+1) and by Tecchiato et al. (2018) for amphibole crystals in equilibrium with Type 2 clinopyroxenes from BA magmas (NNO+0.7 and NNO+1.1). Conversely, rare titanite crystals occur in the groundmass of the enclaves together with Type 3 + plagioclase + titanomagnetite, perhaps indicating slightly higher oxidizing conditions for the EBA products. It has been reported in literature that magnetite and titanite coexist in intermediate to silicic magmas under the effect of increasing buffering conditions from NNO+1 to NNO+2 (Verhoogen 1962; Lipman 1971; Wones, 1981; Nakada 1991).

Magma recharge dynamics and crustal contamination

The textural and compositional changes of clinopyroxenes from crystal-rich enclaves found at CMVD are clear evidence of polybaric crystallization events that took place in geochemically distinct magmas ascending along the plumbing system of the volcano. On one hand, hydrous and least differentiated HMB + BA magmas crystallized olivine + clinopyroxene + amphibole at relatively high pressures under more reduced oxygen fugacity conditions. On the other hand, degassed and highly differentiated EBA magmas ponded at shallow crustal levels, favoring clinopyroxene + plagioclase formation in a more oxidized environment. The crystal cargo from enclaves is characterized by overgrowth features (e.g., Figs. 2, 3a and b, 4c) that are striking evidence of magma recharge dynamics. Oscillatory zoned Type 2 (Fig. 3a and c) testifies to multiple injections of new BA magma batches, segregating from the mafic HMB system after an early fractionation stage of Fo_{84-87} olivine + Cr-spinel + Type 1. In this view, Type 1 represents antecrystic material transported and dispersed in the main BA magma body, where partial resorption phenomena took place (Fig. 2b). In contrast, Type 3 corresponds to the final crystallization stage of EBA magmas, carrying Type 1 + Type 2 antecrysts and xenocrysts (Figs. 2a, 3a and b) while ascending towards the upper parts of the plumbing system. The rare Type 2 overgrowths surrounding Type 3 (Fig. 4c) can be accounted for by the input of EBA into the marginal regions of the BA magma body, in line with the interpretation of Tecchiato et al. (2018).

While the negative trend shown by the $^{87}Sr/^{86}Sr$ vs. Mg# diagram (Fig. 8) may potentially suggest assimilation of crustal material by HMB magma during Type 1 crystallization, the less pronounced variation observed for Type 2 and Type 3 is consistent with negligible BA and EBA interaction with the country rock. This scenario agrees with the AFC (Assimilation and Fractional Crystallization) modeling data derived by Tecchiato et al. (2018), which showed that the ratio of the assimilation rate to the crystallization rate decreases from 0.16 to 0.10 along the overall differentiation path of magma. The broad scattering ($^{87}Sr/^{86}Sr$ = 0.70595-0.70681) of the most primitive (>$Mg\#_{90}$) Type 1 can be plausibly inherited from a mantle source variably contaminated by crustal components. Bulk rock isotopic data from literature (cf. Franciosi et al. 2003; Lustrino et al. 2009) reveal that Sardinian HMB magmas are compositionally heterogeneous ($^{87}Sr/^{86}Sr$ = 0.70399 – 0.70631 and $^{206}Pb/^{204}Pb$ = 18.609 – 18.707) due to the distinctive addition of fluids from both oceanic crust (0.1-0.5%; $^{87}Sr/^{86}Sr$ = 0.70450 and $^{206}Pb/^{204}Pb$ = 18.300) and pelagic sediments (0.035-0.08%; $^{87}Sr/^{86}Sr$ = 0.71985 and $^{206}Pb/^{204}Pb$ = 18.985) to a depleted spinel-bearing mantle wedge ($^{87}Sr/^{86}Sr$ = 0.70250 and $^{206}Pb/^{204}Pb$ = 18.100).

CONCLUDING REMARKS

Clinopyroxene phenocrysts found in crystal-rich enclaves from a basaltic andesitic dome at CMVD have been the object of the present study. Results from detailed petrographic and geochemical analyses lead to the following conclusions:

1. Type 1 + Type 2 clinopyroxenes formed during the differentiation of a HMB parental magma towards BA compositions by olivine + clinopyroxene + amphibole fractionation under high P-H_2O and low-fO_2 conditions;
2. Type 3 clinopyroxene + plagioclase + titanomagnetite cosaturation occurred in a degassed and more evolved EBA magma ponding at shallow crustal level under oxidized buffering conditions;
3. Type 1 + Type 2 clinopyroxenes represent the xenocrystic cargo entrained in the EBA magma during ascent towards the surface;
4. Type 1 isotopic compositions reflect assimilation of crustal material at the early stage of HMB crystallization, whereas Type 2 and Type 3 show limited to negligible interaction of BA and EBA magmas with the country rock;
5. Scattering of isotopic data for Type 1 clinopyroxene phenocrysts with Mg#>90 testifies to the presence of a heterogeneous mantle source.

IMPLICATIONS

Arc magmas are typically produced by the variable contribution of closed- and open-system processes, with the result that the solidified rocks usually contain complex and cryptic information. Geochemical models based on bulk rock data can represent oversimplifications of magmatic processes that may neglect textural evidence of second order mechanisms, preventing a complete understanding of magma chamber dynamics. Our contribution emphasizes the importance of a detailed textural and geochemical investigation on those mineral phases that are stable over a wide range of physico-chemical conditions and, consequently, may be used as proxies for the thorough description of magmatic history. As for the CMVD enclaves, clinopyroxene major, trace, and isotopic compositions may provide reliable insights on the differentiation processes of basaltic to intermediate magmas, especially when crystals belong to the early fractionation of mantle-derived melts in lower crustal environments. The synergy between this methodological approach and the future advancement of analytical techniques is the key to refine our knowledge on the generation and evolution of arc magmas.

ACKNOWLEDGMENTS

This work was supported by the "CRYSTMAG" project, "#000047 Avvio alla Ricerca" project and doctoral scholarship at Sapienza - Università di Roma. We gratefully acknowledge R. Macdonald and H. Downes for their useful and constructive criticisms. The authors also thank C.M. Petrone for her valuable editorial guidance. F. Forni, D. Szymanowski, B. Ellis, M. Guillong, J. Sliwinski, Y. Buret, S. Large, M. Masotta, and M. Nazzari are acknowledged for their precious help, suggestions, and assistance during sample preparation and analytical work. A. Parmigiani is also acknowledged for the logistical support provided during V.T. staying at ETH Zürich.

REFERENCES CITED

Anderson, A.T. (1976) Magma mixing: Petrological process and volcanological tool. Journal of Volcanology and Geothermal Research 1, 3–33.

Armienti, P., Perinelli, and C., Putirka, K.D. (2013) A new model to estimate deep-level magma ascent rates, with applications to Mt. Etna (Sicily, Italy). Journal of Petrology, 54, 795–813.

Avanzinelli, R., Lustrino, M., Mattei, M., Melluso, L., and Conticelli, S. (2009) Potassic and ultrapotassic magmatism in the circum-Tyrrhenian region: Significance of carbonated pelitic vs. pelitic sediment recycling at destructive plate margins. Lithos, 113, 213–227.

Baker, D.R., and Eggler, D.H. (1987) Compositions of anhydrous and hydrous melts coexisting with plagioclase, augite, and olivine or low-Ca pyroxene from 1 atm to 8 kbar; application to the Aleutian volcanic center of Atka. American Mineralogist, 72, 12-28.

Bédard, J.H. (2014) Parameterizations of calcic clinopyroxene-melt trace element partition coefficients. Geochemistry, Geophysics, Geosystems, 15, 303–336.

Berndt, J., Koepke, and J., Holtz, F. (2004) An experimental investigation of the influence of water and oxygen fugacity on differentiation of MORB at 200 MPa. Journal of Petrology, 46, 135-167.

Brotzu, P., Callegari, E., Morra, V., and Ruffini, R. (1997a) The orogenic basalt-andesite suites from the Tertiary volcanic complex of Narcao, SW-Sardinia (Italy): Petrology, geochemistry and Sr-isotope characteristics. Periodico di Mineralogia, 66, 101–150.

Brotzu, P., Lonis, R., Melluso, L., Morbidelli, L., Traversa, G., and Franciosi, L. (1997b) Petrology and evolution of calcalkaline magmas from the Arcuentu volcanic complex (SW Sardinia, Italy). Periodico di Mineralogia, 66, 151–184.

Carminati, E., Lustrino, M., and Doglioni, C. (2012) Geodynamic evolution of the central and western Mediterranean: Tectonics vs. igneous petrology constraints. Tectonophysics, 579, 173–192.

Carroll, M.R., and Rutherford, M.J. (1988) Sulfur speciation in hydrous experimental glasses of varying oxidation state: Results from measured wavelength shifts of sulfur X-rays. American Mineralogist, 73, 845–849.

Cherchi, A., Mancin, N., Montadert, L., Murru, M., Putzu, M.T., Schiavinotto, F., and Verrubbi, V. (2008) The stratigraphic response to the Oligo-Miocene extension in the western Mediterranean from observations on the Sardinia graben system (Italy). Bulletin de la Société Géologique de France, 179, 267–287.

Cioni, R., Marianelli, P., and Santacroce, R. (1998) Thermal and compositional evolution of the shallow magma chambers of Vesuvius: Evidence from pyroxene phenocrysts and melt inclusions, Journal of Geophysical Research: Solid Earth, 103, 277-18, 294.

Clynne, M.A. (1999) A complex magma mixing origin for rocks erupted in 1915, Lassen Peak, California. Journal of Petrology, 40, 105–132.

Conte, A. (1997) Petrology and geochemistry of Tertiary calcalkaline magmatic rocks from the Sarroch district (Sardinia, Italy). Periodico di Mineralogia, 66, 63–100.

Conte, A.M., Palladino, D.M., Perinelli, C., and Argenti, E. (2010) Petrogenesis of the high-alumina basalt-andesite suite from Sant'Antioco Island, SW Sardinia, Italy. Periodico di Mineralogia, 79, 27–55.

Coulon, C., and Baque, L. (1973) Les andésites cénozoïques et les laves associées en Sardaigne Nord-Occidentale (Provinces du Logudoro et du Bosano) - Caractères minéralogiques et chimiques. Contributions to Mineralogy and Petrology, 42, 125-139.

Coulon, C., Demant, A., and Bellon, H. (1974) Premières datations par la méthode K/Ar de quelques laves cénozoïques et quaternaires de Sardaigne Nord-Occidentale. Tectonophysics, 22, 41-57.

Coulon, C., Dostal, J., and Dupuy, C. (1978) Petrology and geochemistry of the ignimbrites and associated lava domes from N.W. Sardinia. Contributions to Mineralogy and Petrology, 68, 89–98.

D'Lemos, R. S. (1996) Mixing between granitic and dioritic crystal mushes, Guernsey, Channel Islands, UK. Lithos, 38, 233–257.

Deriu, M. (1964) Notizie sulla costituzione geologica del Bosano, della Planargia e del Montiferro settentrionale e occidentale, 80 p. Tipografia Bernardi, Parma.

Di Rocco, T., Freda, C., Gaeta, M., Mollo, S., and Dallai, L. (2012) Magma chambers emplaced in carbonate substrate: Petrogenesis of skarn and cumulate rocks and implications for CO_2 degassing in volcanic areas. Journal of Petrology, 53, 2307-2332.

Dieni, I., Massari, F., and Médus, J. (2008) Age, depositional environment and stratigraphic value of the Cuccuru 'e Flores Conglomerate: Insight into the Palaeogene to Early Miocene geodynamic evolution of Sardinia. Bulletin de la Société Géologique de France, 179, 51-72.

Dobosi, G. (1989) Clinopyroxene zoning patterns in the young alkali basalts of Hungary and their petrogenetic significance. Contributions to Mineralogy and Petrology, 101, 112-121.

Dolfi, D., and Trigila, R. (1978) The role of water in the 1944 Vesuvius eruption. Contributions to Mineralogy and Petrology, 67, 297–304.

Downes, H., Thirlwall, M. F., and Trayhorn, S.C. (2001) Miocene subduction-related magmatism in southern Sardinia: Sr–Nd-and oxygen isotopic evidence for mantle source enrichment. Journal of Volcanology and Geothermal Research, 106, 1-22.

Duggen, S., Hoernle, K., van den Bogaard, P., and Garbe-Schönberg, D. (2005) Post-collisional transition from subduction-to intraplate-type magmatism in the westernmost Mediterranean: Evidence for continental-edge delamination of subcontinental lithosphere. Journal of Petrology, 46, 1155-1201.

Dungan, M.A., and Davidson, J. (2004) Partial assimilative recycling of the mafic plutonic roots of arc volcanoes: An example from the Chilean Andes. Geology 32, 773–776.

Eichelberger, J.C. (1980) Vesiculation of mafic magma during replenishment of silicic magma reservoirs. Nature, 288, 446-450.

Foden, J.D., and Green, D.H. (1992) Possible role of amphibole in the origin of andesite: Some experimental and natural evidence. Contributions to Mineralogy and Petrology, 109, 479–493.

Forni, F., Bachmann, O., Mollo, S., and De Astis, G. (2016) The origin of a zoned ignimbrite: Insights into the Campanian Ignimbrite magma chamber (Campi Flegrei, Italy). Earth and Planetary Science Letters, 449, 259–271.

France, L., Ildefonse, B., Koepke, J., and Bech, F. (2010) A new method to estimate the oxidation state of basaltic series from microprobe analyses. Journal of Volcanology and Geothermal Resource, 189, 340–346.

Franciosi, L., Lustrino, M., Melluso, L., Morra, V., and D'Antonio, M. (2003) Geochemical characteristics and mantle sources of the Oligo-Miocene primitive basalts from Sardinia: The role of subduction components. Ofioliti, 28, 105–114.

Frey, H.M., and Lange, R.A. (2011) Phenocryst complexity in andesites and dacites from the Tequila volcanic field, Mexico: Resolving the effects of degassing vs. magma mixing. Contributions to Mineralogy and Petrology, 162, 415–445.

Gaeta, M., Di Rocco, T., and Freda, C. (2009) Carbonate assimilation in open magmatic systems: The role of melt-bearing skarns and cumulate-forming processes. Journal of Petrology, 50, 361-385.

Gori, C., Tribaudino, M., Mantovani, L., Delmonte, D., Mezzadri, F., Gilioli, E., and Calestani, G. (2015) Ca-Zn solid solutions in C2/c pyroxenes: Synthesis, crystal structure, and implications for Zn geochemistry. American Mineralogist, 100, 2209-2218.

Grove, T.L., and Juster, T.C. (1989) Experimental investigations of low-Ca pyroxene stability and olivine-pyroxene-liquid equilibria at 1-atm in natural basaltic and andesitic liquids. Contributions to Mineralogy and Petrology, 103, 287–305.

Guillong, M., Meier, D.L., Allan, M.M., Heinrich, C.A., and Yardley, B.W.D. (2008) SILLS: A MATLAB-based program for the reduction of laser ablation ICP-MS data of homogeneous materials and inclusions. Mineralogical Association of Canada Short Course, 40, 328-333.

Hattori, K. (1996) Occurrence and origin of sulfide and sulfate in the 1991 Mount Pinatubo eruption products. In C.G. Newhall and R.S. Punongbayan, Eds., Fire and Mud: Eruptions and Lahars of Mount Pinatubo, Philippines, p. 807-824. University of Washington Press, Seattle.

Hill, E., Wood, B.J., and Blundy, J.D. (2000) The effect of Ca-Tschermaks component on trace element partitioning between clinopyroxene and silicate melt. Lithos, 53, 203-215.

Humphreys, M.C.S., Blundy, J.D., and Sparks, R.S.J. (2006) Magma evolution and open-system processes at Shiveluch Volcano: Insights from phenocryst zoning. Journal of Petrology 47, 2303–2334.

Humphreys, M.C.S., Edmonds, M., Plail, M., Barclay, J., Parkes, D., and Christopher, T. (2013) A new method to quantify the real supply of mafic components to a hybrid andesite. Contributions to Mineralogy and Petrology, 165, 191–215.

Iezzi, G., Mollo, S., Shahini, E., Cavallo, A., and Scarlato, P. (2014) The cooling kinetics of plagioclase feldspar as revealed by electron-microprobe mapping. American Mineralogist, 99, 898–907.

Jellinek, A.M., Kerr, R.C., and Griffiths, R.W. (1999) Mixing and compositional stratification produced by natural convection. 1. Experiments and their application to Earth’s core and mantle. Journal of Geophysical Research, 104, 7183–7201.

Katsura, T., and Nagashima, S. (1974) Solubility of sulfur in some magmas at 1 atmosphere. Geochimica et Cosmochimica Acta, 38, 517-531.

Lecca, L., Lonis, R., Luxoro, S., Melis, E., Secchi, F., and Brotzu, P. (1997) Oligo-Miocene volcanic sequences and rifting stages in Sardinia: A review. Periodico di Mineralogia, 66, 7–61.

Lipman, P.W. (1971) Iron-titanium oxide phenocrysts in compositionally zoned ash-flow sheets from southern Nevada. The Journal of Geology, 79, 438-456.

Lonis, R., Morra, V., Lustrino, M., Melluso, L., and Secchi, F. (1997) Plagioclase textures, mineralogy and petrology of Tertiary orogenic volcanic rocks from Sindia (central Sardinia). Periodico di Mineralogia, 66, 185–210.

Lustrino, M., Duggen, S., and Rosenberg, C.L. (2011) The Central-Western Mediterranean: Anomalous igneous activity in an anomalous collisional tectonic setting. Earth-Science Reviews, 104, 1-40.

Lustrino, M., Fedele, L., Melluso, L., Morra, V., Ronga, F., Geldmacher, J., Duggen, S., Agostini, S., Cucciniello, C., Franciosi, L., and Meisel, T. (2013) Origin and evolution of Cenozoic magmatism of Sardinia (Italy). A combined isotopic (Sr-Nd-Pb-O-Hf-Os) and petrological view. Lithos, 180–181, 138–158.

Lustrino, M., Morra, V., Fedele, L., and Franciosi, L. (2009) Beginning of the Apennine subduction system in central western Mediterranean: Constraints from Cenozoic "orogenic" magmatic activity of Sardinia, Italy. Tectonics, 28, 1–23.

Lustrino, M., Morra, V., Melluso, L., Brotzu, P., D'Amelio, F., Fedele, L., Franciosi, L., Lonis, R., and Liebercknecht, A.M.P. (2004) The Cenozoic igneous activity of Sardinia. Periodico di Mineralogia, 73, 105–134.

Marks, M., Halama, R., Wenzel, T., and Markl, G. (2004) Trace element variations in clinopyroxene and amphibole from alkaline to peralkaline syenites and granites: Implications for mineral-melt trace-element partitioning. Chemical Geology, 211, 185–215.

Mattioli, M., Guerrera, F., Tramontana, M., Raffaelli, G., and D'Atri, M. (2000) High-Mg Tertiary basalts in Southern Sardinia (Italy). Earth and Planetary Science Letters, 179, 1–7.

McDonough, W.F., Sun, S.S. (1995) The composition of the Earth. Chemical geology, 120, 223-253.

Melekhova, E., Blundy, J., Robertson, R., and Humphreys, M.C.S. (2015) Experimental evidence for polybaric differentiation of primitive arc basalt beneath St. Vincent, Lesser Antilles. Journal of Petrology, 56, 161–192.

Mollo, S., Blundy, J.D., Giacomoni, P., Nazzari, M., Scarlato, P., Coltorti, M., Langone, A., and Andronico, D. (2017) Clinopyroxene-melt element partitioning during interaction between trachybasaltic magma and siliceous crust: Clues from quartzite enclaves at Mt. Etna volcano. Lithos, 284–285, 447–461.

Mollo, S., Forni, F., Bachmann, O., Blundy, J.D., De Astis, G., and Scarlato, P. (2016) Trace element partitioning between clinopyroxene and trachy-phonolitic melts: A case study from the Campanian ignimbrite (Campi Flegrei, Italy). Lithos, 252–253, 160–172.

Mollo, S., Blundy, J. D., Iezzi, G., Scarlato, P., and Langone, A. (2013a) The partitioning of trace elements between clinopyroxene and trachybasaltic melt during rapid cooling and crystal growth. Contributions to Mineralogy and Petrology, 166, 1633-1654.

Mollo, S., Putirka, K., Misiti, V., Soligo, M., and Scarlato, P. (2013b) A new test for equilibrium based on clinopyroxene-melt pairs: Clues on the solidification temperatures of Etnean alkaline melts at post-eruptive conditions. Chemical Geology, 352, 92-100.

Mollo, S., Gaeta, M., Freda, C., Di Rocco, T., Misiti, V., and Scarlato, P. (2010) Carbonate assimilation in magmas: A reappraisal based on experimental petrology. Lithos, 114, 503-514.

Montigny, R., Edel, J.B., and Thuizat, R. (1981) Oligo-Miocene rotation of Sardinia: K-Ar ages and paleomagnetic data of Tertiary volcanics. Earth and Planetary Science Letters, 54, 261–271.

Morgan, D.J., Blake, S., Rogers, N.W., DeVivo, B., Rolandi, G., Macdonald, R., and Hawkesworth, C.J. (2004) Time scales of crystal residence and magma chamber volume from modelling of diffusion profiles in phenocrysts: Vesuvius 1944. Earth and Planetary Science Letters, 222, 933-946.

Morimoto, N. (1988) Nomenclature of Pyroxenes. Mineralogy and Petrology, 39, 55–76.

Morra, V., Secchi, F., Melluso, L., and Franciosi, L. (1997) High-Mg subduction-related Tertiary basalts in Sardinia, Italy. Lithos, 40, 69–91.

Nakada, S. (1991) Magmatic processes in titanite-bearing dacites, central Andes of Chile and Bolivia. American Mineralogist, 76, 548-560.

Nakagawa, M., Wada, K., and Wood, C.P. (2002) Mixed Magmas, Mush Chambers and Eruption Triggers: Evidence from Zoned Clinopyroxene Phenocrysts in Andesitic Scoria from the 1995 Eruptions of Ruapehu Volcano, New Zealand. Journal of Petrology, 43, 2279–2303.

Neave, D.A., and Putirka, K.D. (2017) A new clinopyroxene-liquid barometer, and implications for magma storage pressures under Icelandic rift zones. American Mineralogist, 102, 777-794.

Neumann, H. (1949) Notes on the mineralogy and geochemistry of zinc. Mineralogical Magazine, 28, 575-581.

Parat, F., Holtz, F., and Streck, M.J. (2011) Sulfur-bearing magmatic accessory minerals. Reviews in Mineralogy and Geochemistry, 73, 285-314.

Perinelli, C., Mollo, S., Gaeta, M., De Cristofaro, S.P., Palladino, D.M., Armienti, P., Scarlato, P., and Putirka, K.D. (2016) An improved clinopyroxene-based hygrometer for Etnean magmas and implications for eruption triggering mechanisms. American Mineralogist, 101, 2774-2777.

Pichavant, M., and Macdonald, R. (2007) Crystallization of primitive basaltic magmas at crustal pressures and genesis of the calc-alkaline igneous suite: Experimental evidence from St Vincent, Lesser Antilles arc. Contributions to Mineralogy and Petrology, 154, 535–558.

Pin, C., Briot, D., Bassin, C., and Poitrasson, F. (1994) Concomitant separation of strontium and samarium-neodymium for isotopic analysis in silicate samples, based on specific extraction chromatography. Analytica Chimica Acta, 298, 209–217.

Putirka, K., Johnson, M., Kinzler, R., Longhi, J., and Walker, D. (1996) Thermobarometry of mafic igneous rocks based on clinopyroxene-liquid equilibria, 0-30 kbar. Contributions to Mineralogy and Petrology, 123, 92–108.

Putirka, K.D. (2008) Thermometers and barometers for volcanic systems. Reviews in Mineralogy and Geochemistry, 69, 61–120.

Putirka, K.D., Mikaelian, H., Ryerson, F., and Shaw, H. (2003) New clinopyroxene-liquid thermobarometers for mafic, evolved, and volatile-bearing lava compositions, with applications to lavas from Tibet and the Snake River Plain, Idaho. American Mineralogist, 88, 1542–1554.

Pyle, D.M., Ivanovich, M., and Sparks, R.S.J. (1988) Magma–cumulate mixing identified by U–Th disequilibrium dating. Nature, 331, 157–159.

Ramos, F.C., and Tepley, F.J. (2008) Inter-and intracrystalline isotopic disequilibria: Techniques and applications. Reviews in Mineralogy and Geochemistry, 69, 403-443.

Sas, M., Debari, S.M., Clynne, M.A., and Rusk, B.G. (2017) Using mineral geochemistry to decipher slab, mantle, and crustal input in the generation of high-Mg andesites and basaltic andesites from the northern Cascade Arc. American Mineralogist, 102, 948-965.

Scarlato, P., Mollo, S., Del Bello, E., Von Quadt, A., Richard, J.B., Gutierrez, E., Martinez-Hackert, B., and Papale, P. (2017) The 2013 eruption of Chaparrastique volcano (El Salvador): Effects of magma storage, mixing, and decompression. Chemical Geology, 448, 110-122.

Scarlato, P., Mollo, S., Blundy, J.D., Iezzi, G., and Tiepolo, M. (2014) The role of natural solidification paths on REE partitioning between clinopyroxene and melt. Bulletin of Volcanology, 76, 1–4.

Simonetti, A., Shore, M., and Bell, K. (1996) Diopside phenocrysts from nephelinite lavas, Napak volcano eastern Uganda: Evidence for magma mixing. The Canadian Mineralogist, 34, 411-421.

Singer, B.S., Dungan, M.A., and Layne, G.D. (1995) Textures and Sr, Ba, Mg, Fe, K, and Ti compositional profiles in volcanic plagioclase: Clues to the dynamics of calc-alkaline magma chambers. American Mineralogist, 80, 776–798.

Sparks, R.S.J., and Marshall, L.A. (1986) Thermal and mechanical constraints on mixing between mafic and silicic magmas. Journal of Volcanology and Geothermal Research, 29, 99–124.

Streck, M.J., Dungan, M.A., Malavassi, E., Reagan, M.K., and Bussy, F. (2002) The role of basalt replenishment in the generation of basaltic andesites of the ongoing activity at Arenal volcano, Costa Rica: Evidence from clinopyroxene and spinel. Bulletin of Volcanology, 64, 316–327.

Sun, C., and Liang, Y. (2012) Distribution of REE between clinopyroxene and basaltic melt along a mantle adiabat: Effects of major element composition, water, and temperature. Contributions to Mineralogy and Petrology, 163, 807–823.

Tecchiato, V., Gaeta, M., Mollo, S., Scarlato, P., Bachmann, O., and Perinelli, C. (2018) Petrological constraints on the high-Mg basalts from Capo Marargiu (Sardinia, Italy): Evidence of cryptic amphibole fractionation in polybaric environments. Journal of Volcanology and Geothermal Research, 349, 31–46.

Tuff, J., and Gibson, S.A. (2007) Trace-element partitioning between garnet, clinopyroxene and Fe-rich picritic melts at 3 to 7 GPa. Contributions to Mineralogy and Petrology, 153, 369–387.

Turner, S., George, R., Jerram, D.A., Carpenter, N., and Hawkesworth, C. (2003) Case studies of plagioclase growth and residence times in island arc lavas from Tonga and the Lesser Antilles, and a model to reconcile discordant age information. Earth and Planetary Science Letters, 214, 279–294.

Verhoogen, J. (1962) Distribution of titanium between silicates and oxides in igneous rocks. American Journal of Science, 260, 211-220.

Wones, D.R. (1981) Mafic silicates as indicators of intensive variables in granitic magmas. Mining Geology, 31, 191-212.

Wood, B.J., and Blundy, J.D. (2001) The effect of cation charge on crystal–melt partitioning of trace elements. Earth and Planetary Science Letters, 188, 59–71.

Wood, B.J., and Trigila, R. (2001) Experimental determination of aluminous clinopyroxene-melt partition coefficients for potassic liquids, with application to the evolution of the Roman province potassic magmas. Chemical Geology, 172, 213–223.

FIGURE CAPTIONS

Figure 1. Schematic maps showing the Capo Marargiu Volcanic District (i.e., CMVD), located at about 10 km south-westward of Montresta **(a)**, and the sampling area of the lava dome on the coast of

Cala Bernardu **(b)**. A cliff exposes the inner part of a basaltic andesitic dome hosting abundant crystal-rich enclaves **(c)**. The dome appears as a yellowish, porphyritic rock, whereas the dark-grey enclaves are centimeter-to-meter-sized rounded blocks of crystal-rich material **(d)**.

Figure 2. Textural characteristics of Type 1 clinopyroxene. Type 1 appears as the core of large clinopyroxenes, showing disequilibrium dissolution features predominantly at the sub-rounded edges. Sharp overgrowth textures correspond to Type 3 **(a)** and Type 2 **(b)**. Type 1 crystals usually contain globular inclusions of Fe + Ni + Co sulphides, that likely represent drops of an immiscible liquid **(c)**.

Figure 3. Textural characteristics of Type 2 clinopyroxene. Type 2 occurs as millimeter-sized crystals with a weak reverse oscillatory zoning **(a)** or a spongy cellular texture associated with thick Type 3 overgrowths **(b)**. In some cases, olivine is included in Type 2 crystals **(c)** that, in turn, may be entrapped by large amphiboles **(d)**.

Figure 4. Textural characteristics of Type 3 clinopyroxene. Type 3 is typically found as millimeter-sized glomerocrysts together with plagioclase, titanomagnetite, and rare olivine (**a** and **b**). These clinopyroxenes occasionally show Type 2 overgrowths **(c)**.

Figure 5. Clinopyroxene major element compositions. The Al_{tot} vs. Mg-number and Ti diagrams show that Type 1 and Type 2 evolve along the same path controlled by olivine + clinopyroxene + amphibole fractionation, whereas Type 3 appears as an isolated group of data recording the effect of plagioclase fractionation.

DOI: https://doi.org/10.2138/am-2018-6446

Figure 6. Clinopyroxene trace element composition. The Zn vs Eu/Eu* diagram **(a)** evidences strong and weak Eu anomalies, respectively, for Type 3 and Type 1 + Type 2. The Y vs. Zr diagram **(b)** shows that Type 3 (plagioclase-dominated environment) is characterized by the highest concentrations of incompatible trace elements relative to Type 1 + Type 2 (olivine + clinopyroxene + amphibole - dominated environment).

Figure 7. REE chondrite-normalized (McDonough and Sun, 1995) patterns of clinopyroxenes are bell-shaped, depicting relative depletions in both LREE and HREE with respect to MREE. The REE concentrations increase from Type 1 + Type 2 to Type 3, according to the more differentiated character of the magma.

Figure 8. The $^{87}Sr/^{86}Sr$ vs. Mg# diagram shows that Type 1 isotopic composition is highly variable at the early stage of magma differentiation when both crystal fractionation and assimilation of crustal material occur. In contrast, the $^{87}Sr/^{86}Sr$ ratios of Type 2 and Type 3 do not show significant variations, showing limited to negligible interaction of BA and EBA magmas with the country rock.

Figure 9. The Fe_{tot}^{+2} vs. ΣTs (Ca-Tschermak + Ca-Ti-Tschermak) diagram shows that Type 1 + Type 2 describe a positive linear trend due to crystallization from HMB + BA magmas in water-rich environment (e.g., Dolfi and Trigila 1978). Conversely, Type 3 clinopyroxene and plagioclase cosaturation occur in the degassed EBA magmas, ponding at shallow crustal levels. This feature resembles that observed for clinopyroxenes from other volcanic districts in Sardinia where minerals crystallized at relatively low P-H_2O conditions.

DOI: https://doi.org/10.2138/am-2018-6446

Figure 10. The Al^{IV} vs. Hf and La diagrams show that Type 1 + Type 2 evolve along similar linear paths, accounting for the progressive differentiation of HMB into BA, whereas Type 3 forms an isolated group of data where low Al^{IV} and high Hf and La concentrations indicate crystallization from a compositionally distinct magma under the effect of different environmental conditions.

This is a preprint, the final version is subject to change, of the American Mineralogist (MSA)
Cite as Authors (Year) Title. American Mineralogist, in press.
DOI: https://doi.org/10.2138/am-2018-6446

Figure 1

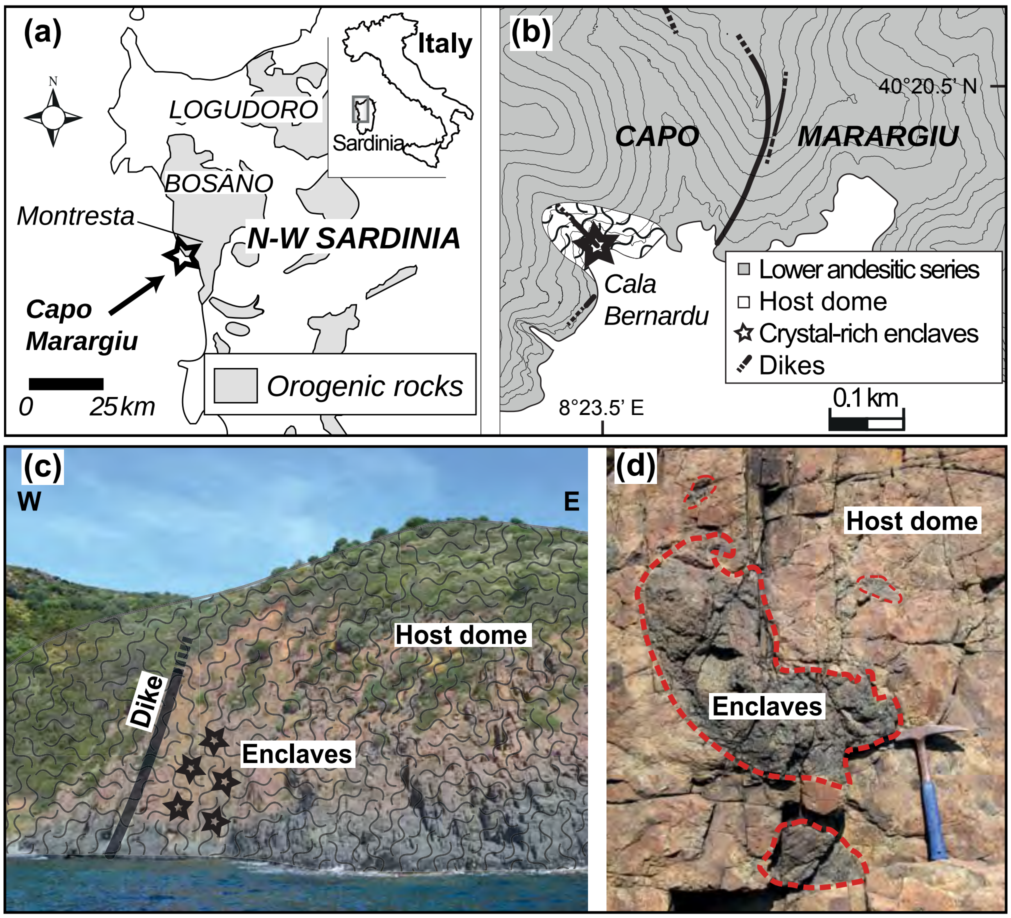

This is a preprint, the final version is subject to change, of the American Mineralogist (MSA)
Cite as Authors (Year) Title. American Mineralogist, in press.
DOI: https://doi.org/10.2138/am-2018-6446

Figure 2

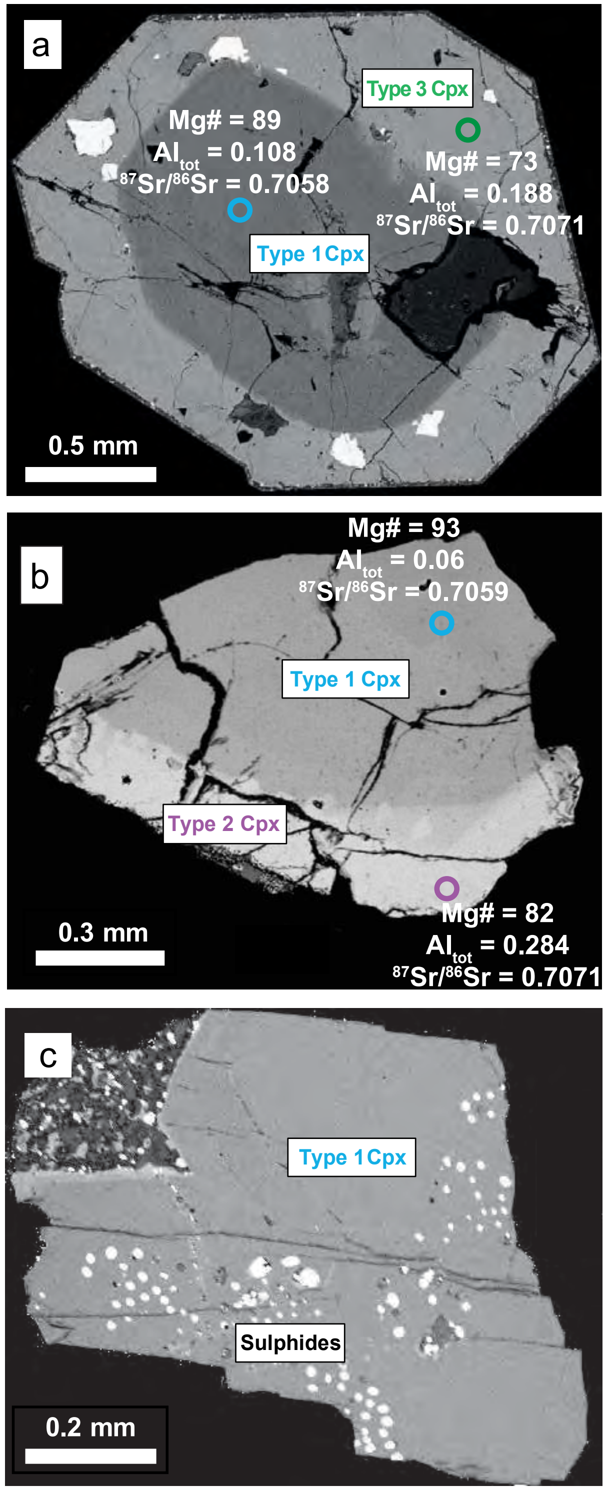

Figure 3

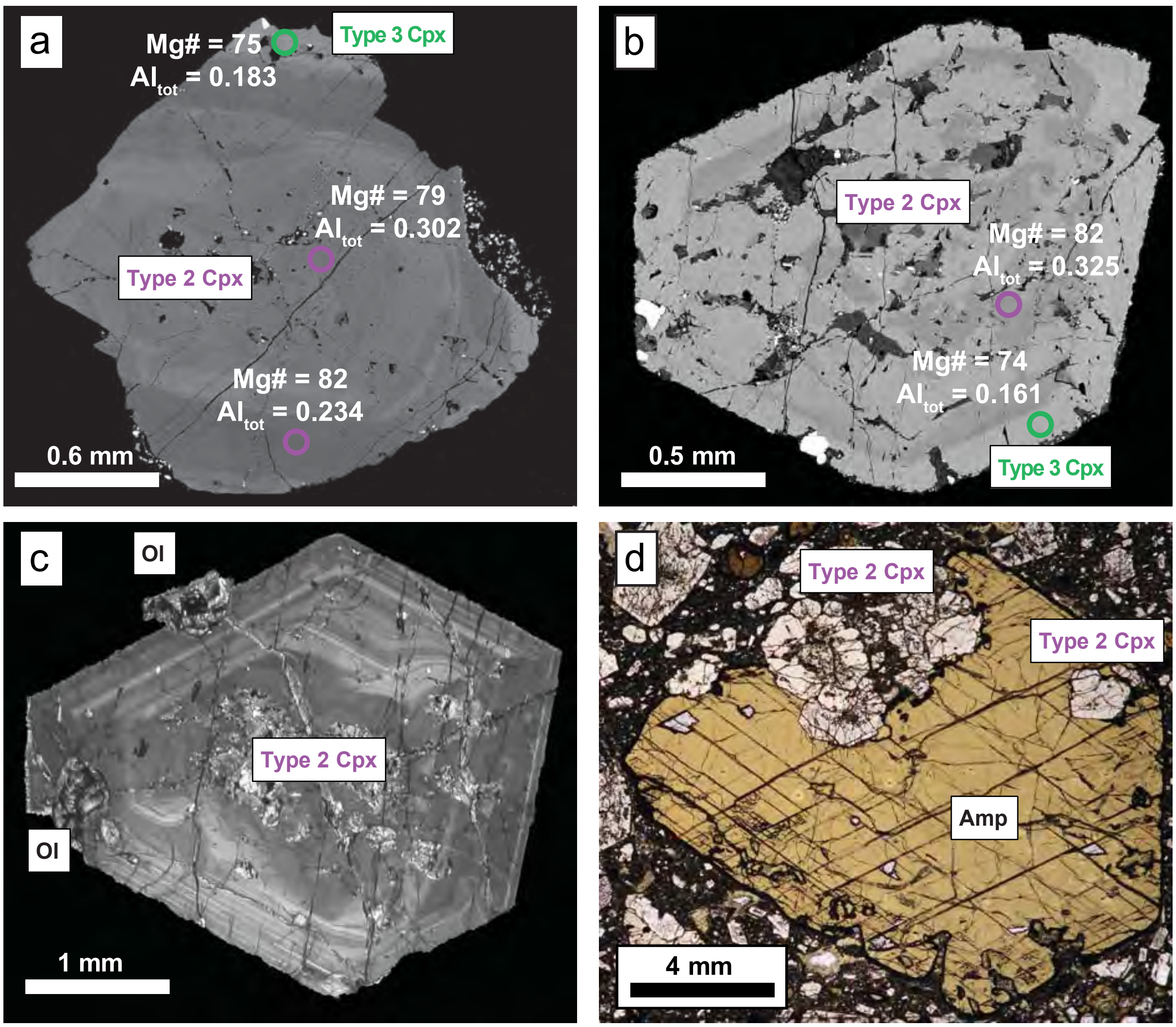
a
Mg# = 75
Al$_{tot}$ = 0.183
Type 3 Cpx
Mg# = 79
Al$_{tot}$ = 0.302
Type 2 Cpx
Mg# = 82
Al$_{tot}$ = 0.234
0.6 mm
b
Type 2 Cpx
Mg# = 82
Al$_{tot}$ = 0.325
Mg# = 74
Al$_{tot}$ = 0.161
Type 3 Cpx
0.5 mm
c
Ol
Type 2 Cpx
Ol
1 mm
d
Type 2 Cpx
Type 2 Cpx
Amp
4 mm

This is a preprint, the final version is subject to change, of the American Mineralogist (MSA)
Cite as Authors (Year) Title. American Mineralogist, in press.
DOI: https://doi.org/10.2138/am-2018-6446

Figure 4

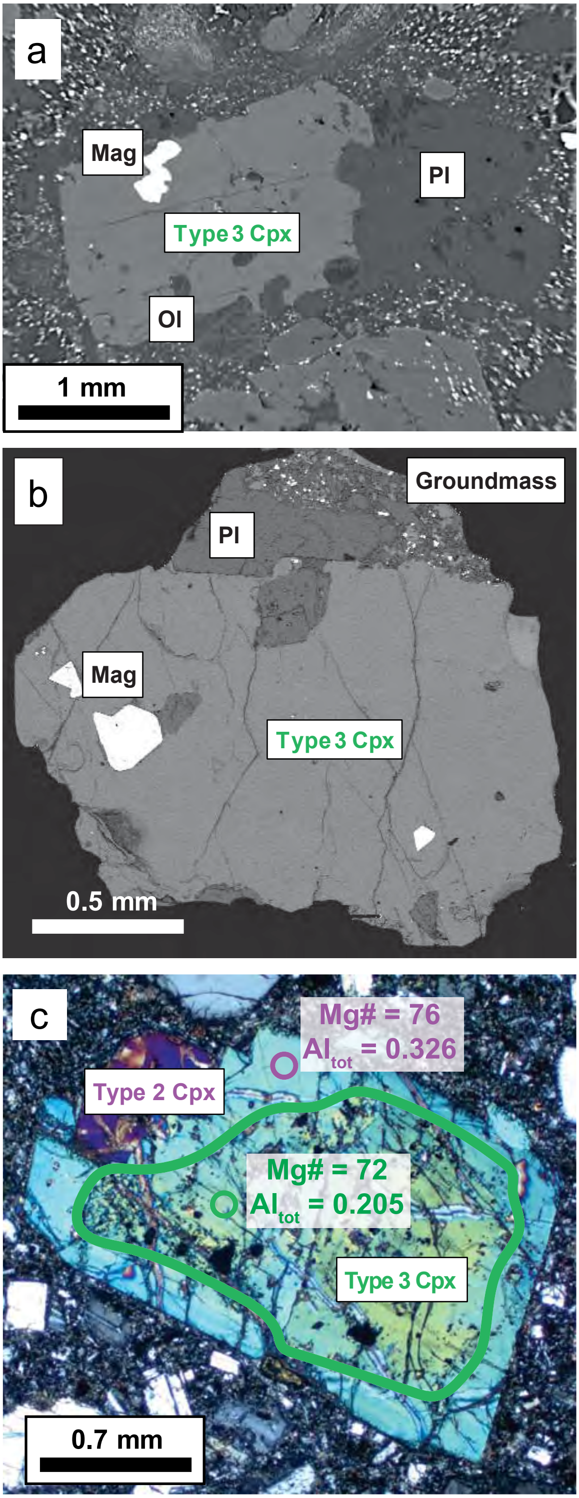

DOI: https://doi.org/10.2138/am-2018-6446

Figure 5

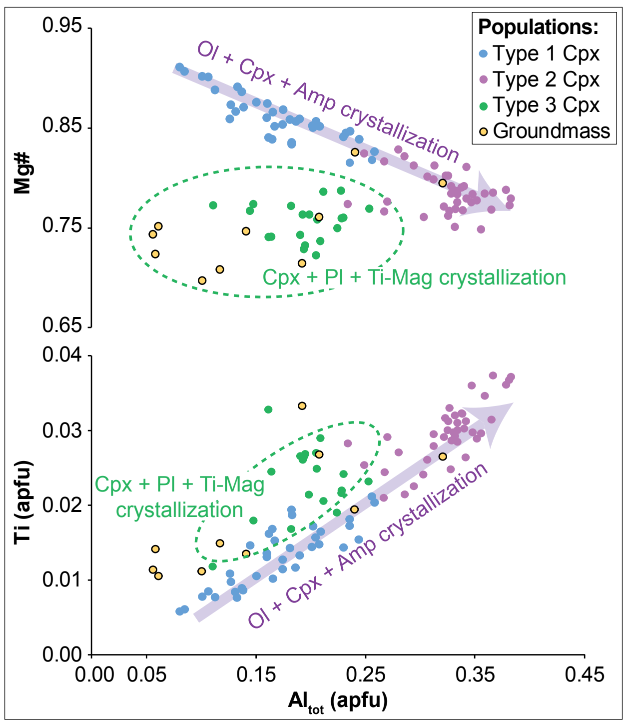

Figure 6

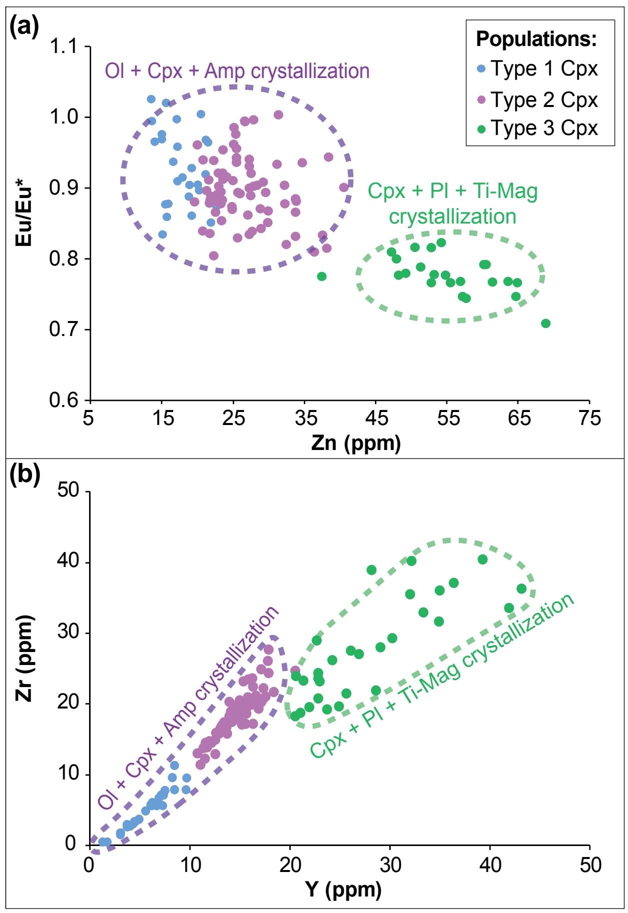
(a)
Populations:
Type 1 Cpx
Type 2 Cpx
Type 3 Cpx
Ol + Cpx + Amp crystallization
Cpx + Pl + Ti-Mag crystallization
Eu/Eu*
Zn (ppm)
1.1
1.0
0.9
0.8
0.7
0.6
5
15
25
35
45
55
65
75
(b)
Ol + Cpx + Amp crystallization
Cpx + Pl + Ti-Mag crystallization
Zr (ppm)
Y (ppm)
50
40
30
20
10
0
0
10
20
30
40
50

Figure 7

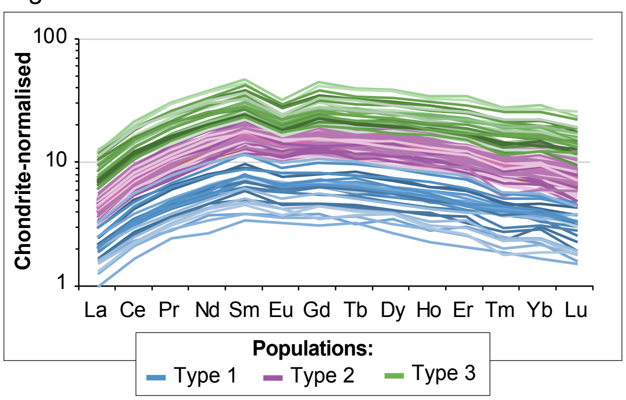
Chondrite-normalised
100
10
1
La
Ce
Pr
Nd
Sm
Eu
Gd
Tb
Dy
Ho
Er
Tm
Yb
Lu
Populations:
Type 1
Type 2
Type 3

This is a preprint, the final version is subject to change, of the American Mineralogist (MSA)
Cite as Authors (Year) Title. American Mineralogist, in press.
DOI: https://doi.org/10.2138/am-2018-6446

Figure 8

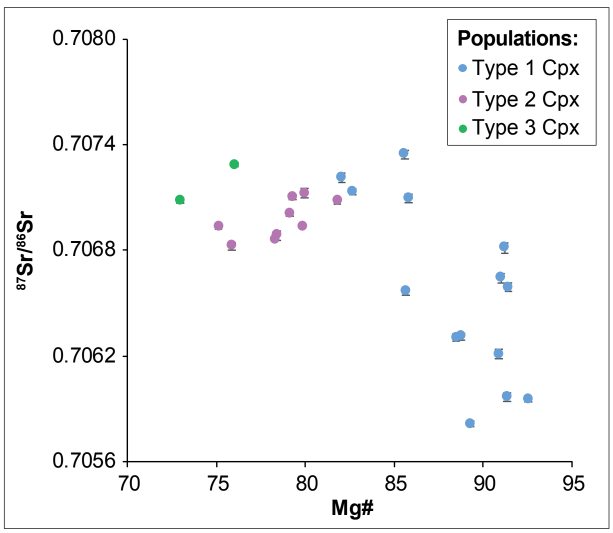

DOI: https://doi.org/10.2138/am-2018-6446

Figure 9

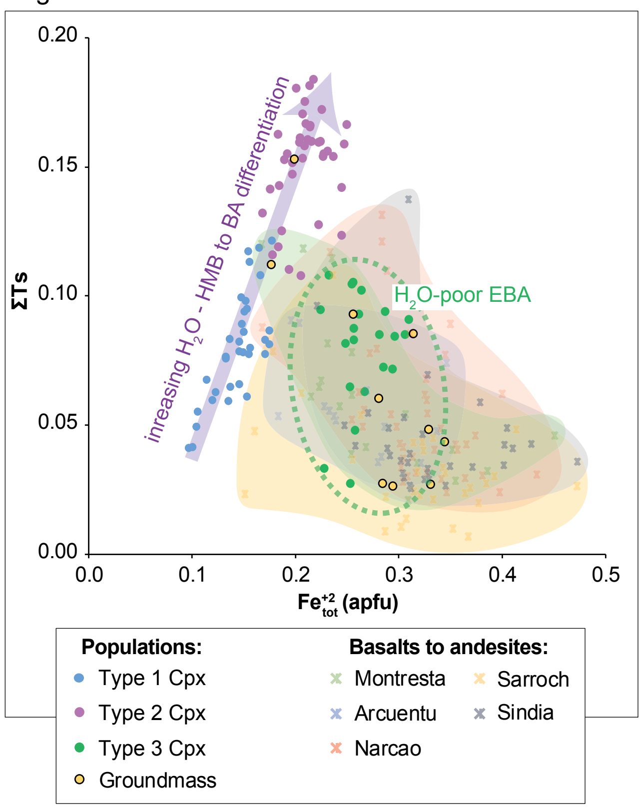

DOI: https://doi.org/10.2138/am-2018-6446

Figure 10